

Routes to identification of intrinsic twist in helical MoS₂ nanotubes by electron diffraction and annular dark-field scanning transmission electron microscopy imaging

A. Mittal,¹ D.-B. Zhang,² C. Teresi,^{1,3} T. Dumitrică,^{2,*} and K. A. Mkhoyan^{1,†}¹*Department of Chemical Engineering and Materials Science, University of Minnesota, Minneapolis, Minnesota 55455, USA*²*Department of Mechanical Engineering, University of Minnesota, Minneapolis, Minnesota 55455, USA*³*School of Materials Science and Engineering, Clemson University, Clemson, South Carolina 29634, USA*

(Received 24 July 2011; published 4 October 2011)

Objective molecular dynamics simulations coupled with a density functional-based tight-binding model indicated that a stress-free single-walled (14,6) MoS₂ nanotube exhibits a torsional deformation of 0.87 deg/nm. Simulated electron diffraction patterns and atomic-resolution annular dark field scanning transmission electron microscopy (ADF-STEM) images of the computed nanotube structures show promise that this peculiar feature can be identified experimentally. The small intrinsic twist removes the translational periodicity prescribed by the rolled-up construction and defines a nanotube for which the atomic order is most fundamentally described by the objective structures concept.

DOI: [10.1103/PhysRevB.84.153401](https://doi.org/10.1103/PhysRevB.84.153401)

PACS number(s): 61.46.Fg, 61.48.De

One of the most promising families of nanoscale materials is single-walled nanotubes (NTs). While identification of chirality in NTs with atomically thin walls such as C NTs¹ and BN NTs^{2,3} has been pursued,^{4,5} little is known about other helical NTs with more complex walls, such as MoS₂, WS₂, and TiS₂.^{6–11} These inorganic NTs have already found many applications, especially related to their mechanical properties¹² and their ability to store hydrogen.¹³ Identification of the equilibrium atomic structure of NTs plays a key role in understanding their structure-property relationships and, therefore, detailed characterization of their natural atomic structures is essential.

The atomic structure of NTs is usually conceptualized by rolling up a flat ribbon into a seamless cylinder. The chiral NT indices (n, m) are used to describe the angle of rolling.¹⁴ In this rolling process, which is associated with pure linear elastic mechanical bending, the circumference vector becomes a circle while the translation vector stays straight. The expectation is that, during the structural optimization, the translational symmetry is preserved. Thus, microscopic treatments formulated under periodic boundary conditions are applied to determine the optimal translational periodicity and the location of atoms in one translational cell. Although not widely used, quantum treatments that make use of helical instead of the translational symmetry are also available.^{15,16} Using objective molecular dynamics¹⁵ (MD) coupled with symmetry-adapted nonorthogonal tight binding¹⁶ implemented in TROCADERO¹⁷ and a density-functional-based tight binding (DFTB) model,^{18,19} we have previously confirmed²⁰ that the rolled-up predictions are also valid in large-diameter chiral MoS₂ NTs. However, under ~ 7 nm in diameter, the rolled-up construction was increasingly inaccurate, especially for near-15° chiral NTs. The rolling-up process becomes nonlinear elastic and the translation vector turns into a helix instead of staying straight. We refer to these structures as NTs with intrinsic twist.

Recently, a variety of structures such as C NTs, viral capsids, and many proteins have been categorized by using the concept of objective structures.²¹ The surprising intrinsic twist result has fundamental implications since it predicts the existence of NTs for which the atomic order is most fundamentally described as an objective structure²¹ rather than

a crystalline one. In this work we actualize these predictions with simulations showing that a careful analysis of the electron diffraction pattern (EDP) obtained from a twisted MoS₂ NT using transmission electron microscopy (TEM) can be a route for proving the existence of the peculiar intrinsic twist effect. Alternatively, if aberration-corrected scanning TEM (STEM) is available, analysis of the annular dark field (ADF) STEM images can be utilized as well.

Objective DFTB simulations with a valence shell basis set comprised of sp and spd functions for the S and Mo atoms, respectively, were performed to obtain the zero-temperature atomic coordinates of MoS₂ NTs with and without intrinsic twist. The current study is focused on a (14,6) MoS₂ NT because its small diameter and nearness to a 15° chirality make it more susceptible to the intrinsic twisting instability.²⁰ Based on the previous structural findings,²⁰ here we carried out microscopic relaxation calculations of this NT described in the “angular-helical” representation^{22–24} from a fundamental objective domain containing one molecule composed of only one Mo and two S atoms. The rolled-up NT is described with^{15,21,23}

$$\mathbf{X}_{j,\zeta_1,\zeta_2} = \mathbf{R}_2^{\zeta_2} \mathbf{R}_1^{\zeta_1} \mathbf{X}_j + \zeta_1 \mathbf{T}_1, \quad j = 1, 2, 3. \quad (1)$$

The rotational matrix \mathbf{R}_2 indicates an angular rotation of angle θ_2 . The rotational matrix \mathbf{R}_1 (of angle θ_1) and the axial vector \mathbf{T}_1 indicate a helical operation. These angular and helical operations have a common axis. The index j runs over the three atoms (the molecule) at locations \mathbf{X}_j inside the fundamental objective domain. Integers ζ_1 and ζ_2 , with $-\infty < \zeta_1 < \infty$ and $\zeta_2 = 0, 1$, label the various replicas of the initial three-atom domain. Ideal values for $\theta_2 = 180^\circ$ and $\theta_1 = 53.54^\circ$ corresponding to the rolled-up construction can be obtained (e.g., by following the approach²² summarized in Ref. 23). First, the NT structure was optimized to identify the optimal $|\mathbf{T}_1|$ value. By keeping θ_1 and θ_2 at their rolled-up predictions, we ensure that the predicted translational periodicity is maintained. 1000 uniformly distributed helical k points and 2 angular numbers were used to converge the band energy. Next, we varied θ_1 to $\theta_1 + \gamma|\mathbf{T}_1|$ in order to determine whether the axial relaxation was sufficient to optimize the structure.

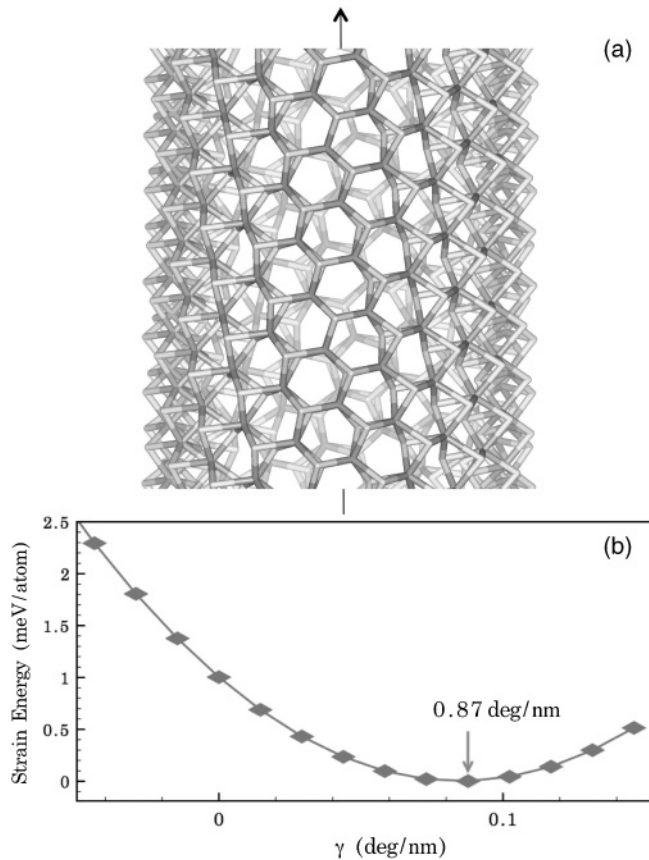


FIG. 1. (a) Stress-free (14,6) MoS₂ NT. Light gray is S and gray is Mo. (b) Strain energy as a function of twist rate. The arrow points to the energy minimum corresponding to the stress-free structure with intrinsic twist.

The results presented in Fig. 1 demonstrate that, when the twist rate γ is varied, the stable minimum of the structure does not correspond to $\gamma = 0$ deg/nm. Variations in θ_1 lower the energy of the structure, which finally achieves a stress-free state with a residual twist of 0.87 deg/nm. This is in agreement with our previous objective MD simulations carried out on a larger objective domain.

Two existing TEM techniques can be employed to observe the intrinsic twist in MoS₂ NTs: electron diffraction and atomic-resolution imaging. Other techniques that are used to identify the (n,m) indices of NTs, such as Raman spectroscopy²⁵ and scanning tunneling microscopy (STM),⁴ appear to be at a disadvantage. The intrinsic twist does not change the (n,m) indices and the applicability of Raman spectroscopy to identify small torsional deformation is untested. The wall of an MoS₂ NT is actually a complex three-atomic-layer system [Fig. 1(a)] and the use of STM for structural characterization becomes less reliable.

Electron diffraction has previously been used for characterization of NTs^{1,26} and especially for structural features caused by different chiral arrangements.^{18,27} For instance, the existence of armchair and zigzag MoS₂ NTs was confirmed by comparing experimental EDPs with simulated ones.¹⁸ Chiral indices of a variety of C NTs have been determined by electron diffraction analysis.^{4,28,29} The chirality of various

NTs, including Au and Ag-alloyed MoS₂ and WS₂, has also been studied by electron diffraction.⁷

To determine if there are substantial differences between the EDPs of MoS₂ NTs with and without twist, here we simulated EDPs of both types of NTs using the MULTISLICE programs developed by Kirkland³⁰ and based on the algorithm introduced by Cowley and Moodie.³¹ Models of 20-nm-long (14,6) MoS₂ NTs were constructed using atomic coordinate files obtained via microscopic calculations discussed earlier. A grid of 2048 × 2048 pixels with a reciprocal pixel size of 0.045 nm⁻¹ was used in these simulations. A 100 keV electron beam incident normal to the NT axis was used because this is the most common orientation of NTs in an experimental setup. Propagation of the electron beam through the entire specimen was achieved by passing the beam through 1 Å slices. The effect of temperature was modeled by averaging 20 frozen phonon configurations at 298 K. Root-mean-square displacements of 0.071 and 0.045 Å were used for S and Mo atoms, respectively, which were obtained from the corresponding Debye-Waller factors for similar MoS₂ compounds.³² Nonphysical high-frequency artifacts were filtered out by convoluting the EDPs with a Gaussian function with a standard deviation of 0.045 nm⁻¹.

EDPs of (14,6) MoS₂ NTs with and without twist are shown on a logarithmic scale in Figs. 2(a) and 2(b). The diffraction spots are elongated due to the cylindrical structure of the NT.²⁷ EDPs from NTs show $mm2$ symmetry in $(hk0)$ spots.¹ As only $(hk0)$ spots are present in the EDP of a single-wall NT, the analysis of one quadrant of the EDP is sufficient for identifying differences. To characterize the differences between diffraction spots, the distance between the equatorial line and each diffraction spot was measured, as shown in Fig. 2(a), and the results are tabulated in Table I. The error in the position of the diffraction spot was estimated by measuring the variation in the position of the peak intensity of the diffraction spot at different locations along the elongated spot. A maximum variation of ± 0.05 nm⁻¹ was observed. The range of diffraction spot position among the 20 frozen phonon configurations was less than 0.0018 nm⁻¹, which is significantly lower than the sampling error. The largest difference in the positions of diffraction spots obtained from (14,6) MoS₂ NT with and without twist was 0.09 nm⁻¹ and that was observed for spots D_3 and A_1 . The difference is clearly above the error level and, therefore, can be used to identify presence of the intrinsic twist.

Additional EDPs of $(14 \pm 1, 6 \pm 1)$ MoS₂ NTs [i.e., (15,6), (13,6), (14,5), and (14,7) NTs] were simulated [see Figs. 2(c)–2(f)], in order to ensure that the above differences in EDPs due to the presence of an intrinsic twist can be distinguished from those due to small changes in chiral indices. The intrinsic twist was not considered in these additional NTs. As can be observed in Table I, the differences between D_i ($i = 1, 2, 3$) and A_1 values for (14,6) and other chiral NTs are considerably larger than between those from (14,6) NTs with and without intrinsic twist. Thus, the intrinsic twist cannot be confused with other chiral NTs.

Atomic resolution ADF-STEM images can be alternatively used to detect the intrinsic twist. Unlike conventional bright-field TEM imaging, ADF-STEM imaging avoids complications in image interpretation due to focusing conditions.

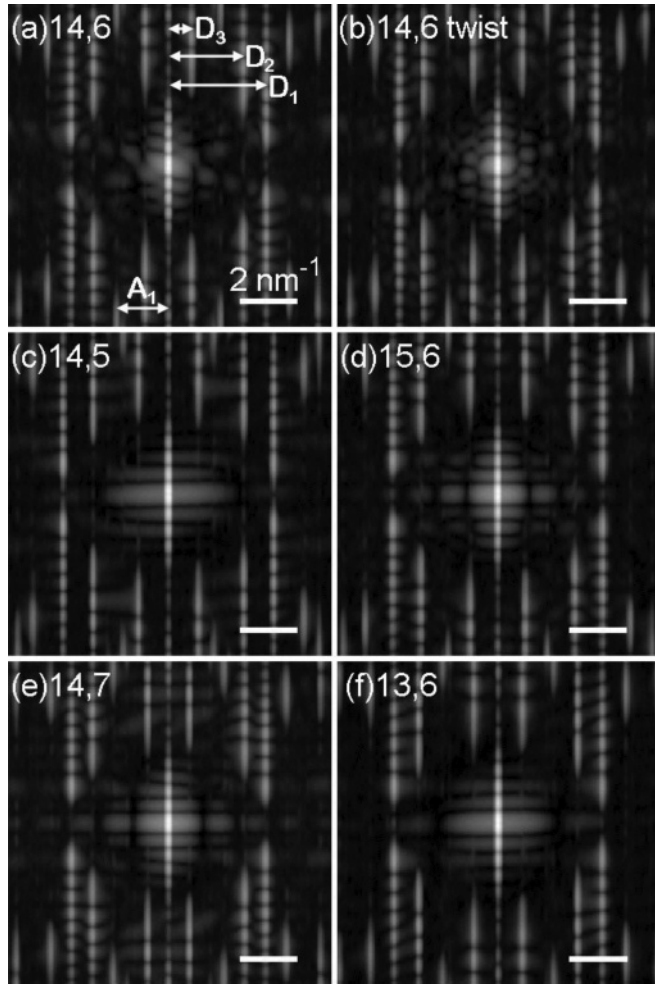


FIG. 2. EDPs of different MoS₂ NTs: (a) (14,6), (b) (14,6) NT with intrinsic twist, (c) (14,5), (d) (15,6), (e) (14,7), and (f) (13,6). EDPs are shown on a logarithmic scale.

Here, ADF-STEM image intensity is directly dependent on the atomic number of the scattering atom.^{33,34} Simulations of ADF-STEM images were carried out using the same MULTISLICE code used above to simulate EDPs. The probe parameters used in simulations were 100 keV incident beam energy, $C_{s(3)} = -0.015$ mm and $C_{s(5)} = 10$ mm for spherical aberration coefficients, $\Delta f = -30$ Å for defocus, and $\alpha_{\text{obj}} = 25$ mrad for the objective aperture, which provide a converged probe with a full width at half maximum (FWHM)

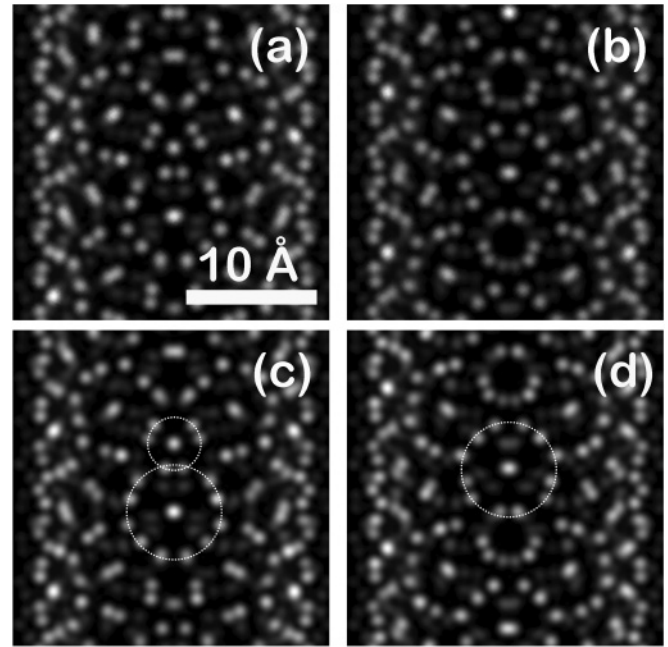


FIG. 3. ADF-STEM images of MoS₂ (14,6) NT (a) without and (b) with intrinsic twist. (c), (d) ADF-STEM images of the same tubes as in (a) and (b), respectively, after rotating NTs by 15° along the tube axis.

of 0.8 Å.^{35,36} The images were calculated with a 7.4 pixel/Å sampling.

Simulated atomic resolution ADF-STEM images of characteristic sections of (14,6) MoS₂ NTs with and without intrinsic twist are shown in Figs. 3(a) and 3(b). The projected positions of the Mo and S atoms in most cases can be identified: Mo atoms as bigger and brighter spots and S atoms as smaller and dimmer spots. In an actual experiment the exact orientation of the suspended NT relative to the incident beam is difficult to control. Therefore, to understand the effects on images of NT rotation relative to its axis, we also simulated ADF-STEM images of the same NTs after rotating both of them by 15°. The resulting images are presented in Figs. 3(c) and 3(d), respectively. As can be seen, the rotation along the tube axis is equivalent to a shift in the imaging area. Specifically, a 15° rotation corresponds to a 2.1 Å shift.

The simulated ADF-STEM image of a (14,6) MoS₂ NT without intrinsic twist has two bright spots in the middle of the NT, highlighted by dotted circles, while the ADF-STEM

TABLE I. Distances between diffraction spots and equatorial line for different NTs.

NT	Distance from Equatorial Line (nm ⁻¹) ± 0.05 nm ⁻¹			
	D_1	D_2	D_3	A_1
(14,6) Twisted	3.33	2.57	0.77	1.71
(14,6)	3.38	2.57	0.86	1.80
(14,5)	3.65	2.61	1.04	2.07
(15,6)	3.65	2.66	0.95	1.71
(14,7)	3.33	2.61	0.72	1.89
(13,6)	3.60	2.75	0.86	1.89

image of (14,6) MoS₂ NT with intrinsic twist is missing a bright spot in one of these locations [cf. Figs. 3(c) and 3(d)]. Comparison with atomic models shows that the bright spot in the larger circle corresponds to the projected image of two Mo atoms and the bright spot in the smaller circle corresponds to the projected image of four sulfur atoms. Such distinctive features provide an alternate route for identifying the intrinsic twist.

In conclusion, our simulations presented herein show that, in spite of the small diameter and the complexity of the MoS₂ wall, the atomic-scale intrinsic twist in an MoS₂ NT predicted by simulations could be observed in experiment by either electron diffraction using conventional TEM or atomic-resolution ADF-STEM imaging using aberration-corrected STEM. We envision that these techniques can be utilized in

other small-diameter chiral NTs predicted to exhibit intrinsic twists of similar magnitude, such as C NTs,^{24,37} BN NTs,³⁷ and TiS₂ NTs.³⁸

We thank G. Seifert for providing the MoS₂ DFTB parameters. This work was partially supported by the NSF MRSEC program DMR-0819885 and the Abu Dhabi-Minnesota Institute for Research Excellence (ADMIRE), a partnership between the Petroleum Institute of Abu Dhabi and the Department of Chemical Engineering and Materials Science of the University of Minnesota. D.-B.Z and T.D. thank NSF CAREER Grant CMMI-0747684 and AFOSR Grant FA9550-09-1-0339. Computational resources from the University of Minnesota Supercomputing Institute were used.

*td@me.umn.edu

†mkhoyan@umn.edu

¹S. Iijima, *Nature (London)* **354**, 56 (1991).

²N. G. Chopra, R. J. Luyken, K. Cherrey, V. H. Crespi, M. L. Cohen, S. G. Louie, and A. Zettl, *Science* **269**, 966 (1995).

³D. Golberg, Y. Bando, Y. Huang, T. Terao, M. Mitome, C. C. Tang, and C. Y. Zhi, *ACS Nano* **4**, 2979 (2010).

⁴A. Jurio, M. Dresselhaus, and G. Dresselhaus, *Carbon Nanotubes* (Springer, Berlin, 2008).

⁵H. Lin, J. Lagoute, V. Repain, C. Chacon, Y. Girard, F. Ducastelle, H. Amara, A. Loiseau, P. Hermet, L. Henrard, and S. Rousset, *Phys. Rev. B* **81**, 235412 (2010).

⁶P. Santiago, J. A. Ascencio, D. Mendoza, M. Perez-Alvarez, A. Espinosa, C. Reza-SanGermaan, P. Schabes-Retchkiman, G. A. Camacho-Bragado, and M. Jose-Yacamaan, *Appl. Phys. A* **78**, 513 (2004).

⁷M. Remskar, Z. Skraba, P. Stadelmann, and F. Levy, *Adv. Mater.* **12**, 814 (2000).

⁸M. Remskar, A. Mrzel, Z. Skraba, A. Jseih, M. Ceh, J. Demsar, P. Stadelmann, F. Levy, and D. Mihailovic, *Science* **292**, 479 (2001).

⁹Y. Feldman, E. Wasserman, D. J. Srolovitz, and R. Tenne, *Science* **267**, 222 (1995).

¹⁰K. S. Coleman, J. Sloan, N. A. Hanson, G. Brown, G. P. Clancy, M. Terrones, H. Terrones, and M. L. H. Green, *J. Am. Chem. Soc.* **124**, 11580 (2002).

¹¹J. Chen, Z.-L. Tao, S.-L. Li, X.-B. Fan, and S.-L. Chou, *Adv. Mater.* **15**, 1379 (2003).

¹²R. Tenne and C. N. R. Rao, *Philos. Trans. R. Soc. London A* **362**, 2099 (2004).

¹³J. Chen, S.-L. Li, Z.-L. Tao, Y.-T. Shen, and C.-X. Cui, *J. Am. Chem. Soc.* **125**, 5284 (2003).

¹⁴R. Saito, G. Dresselhaus, and M. S. Dresselhaus, *Physical Properties of Carbon Nanotubes* (Imperial College Press, London, 1998).

¹⁵T. Dumitrică and R. D. James, *J. Mech. Phys. Solids* **55**, 2206 (2007).

¹⁶D.-B. Zhang, M. Hua, and T. Dumitrică, *J. Chem. Phys.* **128**, 084104 (2008).

¹⁷R. Rurali and E. Hernandez, *Comp. Mat. Sci.* **28**, 85 (2003).

¹⁸G. Seifert, H. Terrones, M. Terrones, G. Jungnickel, and Th. Frauenheim, *Phys. Rev. Lett.* **85**, 146 (2000).

¹⁹I. Milosevic, B. Nikolic, E. Dobardzic, M. Damjanovic, I. Popov, and G. Seifert, *Phys. Rev. B* **76**, 233414 (2007).

²⁰D.-B. Zhang, T. Dumitrică, and G. Seifert, *Phys. Rev. Lett.* **104**, 065502 (2010).

²¹R. D. James, *J. Mech. Phys. Solids* **54**, 2354 (2006).

²²Ge. G. Samsonidze, R. Saito, A. Jorio, M. A. Pimenta, A. G. Souza Filho, A. Gruneis, G. Dresselhaus, and M. S. Dresselhaus, *J. Nanosci. Nanotech.* **3**, 431 (2003); E. B. Barros, A. Jorio, Ge. G. Samsonidze, R. B. Capaz, A. G. Souza Filho, J. Mendes Filho, G. Dresselhaus, and M. S. Dresselhaus, *Phys. Rep.* **431**, 261 (2006).

²³D.-B. Zhang and T. Dumitrică, *Appl. Phys. Lett.* **93**, 031919 (2008).

²⁴D. G. Vercosa, E. B. Barros, A. G. Souza Filho, J. Mendes Filho, Ge. G. Samsonidze, R. Saito, and M. S. Dresselhaus, *Phys. Rev. B* **81**, 165430 (2010).

²⁵N. Anderson, A. Hartschuh, and L. Novotny, *Nano Lett.* **7**, 577 (2007).

²⁶R. Tenne, L. Margulis, M. Genut, and G. Hodes, *Nature (London)* **360**, 444 (1992).

²⁷J. C. Meyer, M. Paillet, G. S. Duesberg, and S. Roth, *Ultramicroscopy* **106**, 176 (2006).

²⁸Z. Liu and L. Qin, *Chem. Phys. Lett.* **408**, 75 (2005).

²⁹H. Deniz, A. Derbakova, and L.-C. Qin, *Ultramicroscopy* **111**, 66 (2010).

³⁰E. J. Kirkland, *Advanced Computing in Electron Microscopy*, 2nd ed. (Springer, New York, 2010).

³¹J. M. Cowley and A. F. Moodie, *Acta. Cryst.* **10**, 609 (1957).

³²P. Afanasiev and I. Bezverkhy, *Chem. Mater.* **14**, 2826 (2002).

³³E. J. Kirkland, R. F. Loane, and J. Silcox, *Ultramicroscopy* **23**, 77 (1987).

³⁴S. J. Pennycook and L. A. Boatner, *Nature (London)* **336**, 565 (1988); S. J. Pennycook, *Ultramicroscopy* **30**, 58 (1989).

³⁵K. A. Mkhoyan, P. E. Batson, J. Cha, W. J. Schaff, and J. Silcox, *Science* **312**, 1354 (2006).

³⁶K. A. Mkhoyan, S. E. Maccagnano-Zacher, E. J. Kirkland, and J. Silcox, *Ultramicroscopy* **108**, 791 (2008).

³⁷D.-B. Zhang, E. Akatyeva, and T. Dumitrică, *Phys. Rev. B* **84**, 115431 (2011).

³⁸D. Teich, T. Lorenz, J.-O. Joswig, G. Seifert, D.-B. Zhang, and T. Dumitrică, *J. Phys. Chem. C* **115**, 6392 (2011).